

# We are IntechOpen, the world's leading publisher of Open Access books Built by scientists, for scientists

6,900

Open access books available

186,000

International authors and editors

200M

Downloads

Our authors are among the

154

Countries delivered to

TOP 1%

most cited scientists

12.2%

Contributors from top 500 universities



WEB OF SCIENCE™

Selection of our books indexed in the Book Citation Index  
in Web of Science™ Core Collection (BKCI)

Interested in publishing with us?  
Contact [book.department@intechopen.com](mailto:book.department@intechopen.com)

Numbers displayed above are based on latest data collected.  
For more information visit [www.intechopen.com](http://www.intechopen.com)



---

# Detection Methods of Nanoparticles in Plant Tissues

---

An Yan and Zhong Chen

Additional information is available at the end of the chapter

<http://dx.doi.org/10.5772/intechopen.74101>

---

## Abstract

The increasing use of nanoparticles (NPs) in the world has raised significant concerns about their potential impacts on ecosystems, food safety and human health, leading to an emerging research theme about the interaction between crop plants and NPs. Therefore, a full understanding of plant-NP interaction and phytotoxicological mechanism is required for accurate risk assessment to ensure the safe use of nanoparticle. A range of analytical techniques have been developed to detect and characterize the uptake, translocation, cellular internalization and intracellular biotransformation of nanoparticles in plants. Imaging methodologies, including various electron microscopy, spectrometry-based techniques, together with ICP-based techniques such as ICP-OES, ICP-MS and SP-ICP-MS, have been widely used to obtain information about NPs size, morphology, size distribution, cellular localization, elemental speciation, mass concentration and so on. Due to the complexity of biological samples to be analyzed, these techniques are often combined accordingly to provide complementary information regarding plant-NP interaction. This review provides an introduction to the most widely used techniques in the study of interactions between plants and nanoparticles. In addition, applications of these techniques in the study of plant-NP interaction from recent works are exemplified to illustrate how the understanding of plant-NP interaction is achieved through these techniques.

**Keywords:** nanoparticles, microscopy, X-ray, mass spectrometry, plant, uptake, biotransformation

---

## 1. Introduction

Over the past decades, nanotechnology has been widely applied on commercial products on the market, including biosensor, catalysts to optics, antimicrobial activity, computer transistors, electrometers, and wireless electronic logic and memory schemes. In the agriculture

sector, nanoparticles are often incorporated into nano-formulated pesticides, fertilizers, and nanobiosensors for crop protection [1]. Therefore, the application of engineered nanomaterials worldwide inevitably caused the release and accumulation of nanoparticles in the environment [2].

As the basic components of the ecosystem, plants are sessile and their roots absorb nutrients and water as well as contaminants from their environment. Accumulating evidence demonstrated that engineered nanoparticles could be released from some commercial products, further be taken in and accumulated in plant tissues. As plants may serve as a potential pathway for the transportation of nanoparticles through the food chain [3], the increasing applications of engineered nanomaterials in the world have raised a growing concern about their potential adverse impacts on ecosystems, food safety and human health [2, 4]. Therefore, to evaluate potential environmental risks imposed by nanoparticle application, it is important to understand the interaction between nanoparticles and plants, as well as NP's behavior and toxicity in plants. However, the behavior of NPs in plants and phytotoxicity mechanism are so complicated that contradictory results regarding the effects of nanoparticles on plants were obtained from various studies during the past decade [5–9]. These conflicting results indicate that impacts of nanoparticles on plants largely depend on the type and concentration of nanoparticles, plants species, tissue exposed, and the experimental conditions [6, 10, 11].

There are various engineered nanoparticles with different size, morphology, and properties. Engineered nanoparticles also exhibit distinct physical and chemical properties with different environmental behaviors and toxicity in comparison with their bulk counterparts, which could be attributed to the small size at nanoscale (1–100 nm) and high surface-to-volume ratios of nanoparticles [12]. Upon nanoparticle exposure, the directly contact between nanoparticles and roots leads to the uptake of nanoparticles by roots and translocation of nanoparticles in plants [10, 13]. Different types of nanoparticles exhibit distinct behaviors and translocation characteristics. During interaction with biological environments, nanoparticles can also be transformed by plants, which in turn alter environmental fate and toxic properties of nanoparticles [14, 15]. Therefore, the toxic effect and behavior of nanoparticles are determined by not only the initial properties (such as particle size, shape, structure, charge, elemental composition, mass concentration, and state of aggregation etc.), but also by the physicochemical evolution [16–18]. Hence, in order to accurately assess the phytotoxicity of nanoparticles, it is necessary to determine the original characteristics of NPs before treatment, uptake and translocation, cellular internalization and intracellular biotransformation during interaction with plants.

Approaches to detect and characterize NPs during plant-NP interaction are thus becoming crucial in our studies. Nowadays, a variety of analytical techniques have been developed to provide the necessary information regarding plant-NP interaction, including microscopy imaging, chromatography, spectrometry-based techniques, and so on. In this review, we describe the advantages and limitations of a selection of current most frequently-used methods in the study of uptake, distribution, translocation and biotransformation of NPs in plants. We also exemplify the usage of these analytical techniques with instances from recent studies.

## 2. Techniques for nanoparticle detection

### 2.1. Imaging techniques

#### 2.1.1. *Transmission electron microscopy/scanning electron microscopy*

Transmission electron microscopy (TEM) and scanning electron microscopy (SEM) are considered to be the most popular techniques for the analysis of nanomaterials. Electron microscopy straightforwardly captures projected area of the particles, providing visualization of true particle size dimensions.

In TEM process, a focused electron beam is transmitted through a specimen, an image is formed from the interaction of the electrons with the sample. The image is then magnified and focused onto an imaging device. TEM is capable of imaging at a significantly higher resolution (down to the sub-nanometer) than light microscopes, it can visualize as small as a single column of atoms, which is thousands of times smaller than a resolvable object seen in a light microscope.

In SEM process, a focused beam of electrons scans the surface of the sample; interaction between electrons and atoms in the surface of sample produces various signals that contain information about the sample's surface topography and composition. Then an image is formed upon focusing of scattered electrons. SEM can achieve resolution better than 1 nm [19]. It can be used to image intact sample as well as sectioned sample [15].

Through visualization of nanoparticle position within a cell or tissue, TEM/SEM can provide the precise nanoparticle information about their size, structure, shape, morphology, dispersion or aggregation state, which is informative for assessing in vitro nanoparticle uptake and localization. Nanoparticle sizes are calculated and expressed as a sphere diameter having a similar projected area as the projected image of the nanoparticle. Particle size analysis is carried out by manually using a marking device to move along the nanoparticles. A mean linear dimensional measure of the nanoparticles is obtained by dividing the total length of the nanoparticles by the total number of nanoparticles counted [20]. In addition, when combined with spectroscopic methods, characterization of the composition of the internalized nanoparticles became possible [21]. Owing to the high lateral resolution of TEM, it could also be used to trace the dynamics of individual NPs in a living cell or plant tissues.

#### 2.1.2. *Scanning transmission electron microscope*

Scanning transmission electron microscope (STEM) is a type of transmission electron microscope (TEM). A typical STEM is a conventional TEM equipped with additional scanning coils, detectors and necessary circuitry. Like a conventional TEM, images are formed by electrons transmitting through a thin specimen. The difference is that in STEM the electron beam is focused to a fine spot (with spot size 0.05–0.2 nm), then it scans over the sample in a raster. The rastering of the beam across the sample makes STEM suitable for combination with analytical techniques such as annular dark-field imaging and spectroscopic mapping, to obtain

information on the structure of nanoparticles with sub-nanometer resolution and their chemical composition [22, 23].

Dark-field microscopy with a STEM, such as high-angle annular dark field scanning transmission electron microscopy (HAADF-STEM), can be used to distinguish elements with high atomic number (Ag, Au, etc.) from the major elements in organisms (C, N, O, etc.) with a high spatial resolution (down to 1 nm) [24].

### 2.1.3. *Dynamic light scattering*

Dynamic light scattering (DLS) technique is the most commonly employed high-throughput technique to measure nanoparticle size and determine aggregation state of nanoparticles in aqueous suspensions. In DLS analysis, the Brownian movements of the NPs in aqueous suspensions cause constructive and destructive interference, which results in time-dependent fluctuations in scattering intensity. Then the average particle size can be calculated from these time-dependent fluctuations in scattering intensity by application of the autocorrelation function and subsequent calculation of the exponential decay [25]. Meanwhile, the zeta potential, a key indicator of the stability of colloidal dispersions, is measured rapidly using DLS. DLS is able to analyze samples containing very broad distributions of species; it can also detect very small amounts of the higher mass species [25].

### 2.1.4. *Energy-dispersive X-ray spectroscopy*

Energy-dispersive X-ray spectroscopy (EDS) is used as an analytical technique to analyze a sample's elemental composition or chemical characterization. EDS applies a high-energy electron beam which focuses into the sample of interest to excite in an inner shell an electron and to eject it from the shell, thus generating an electron hole. Then an electron from the outer shell with higher-energy fills the hole, which releases the energy in difference in between the outer shell and the inner shell in the form of X-ray [26]. As each element has a unique set of peaks on electromagnetic emission spectrum determined by its unique atomic structure, through measuring the number and energy of the X-rays emitted from the sample by an EDS instrument, the information about elemental composition of the sample is obtained [26].

### 2.1.5. *X-ray absorption and X-ray fluorescence*

There are two main types of X-ray spectroscopy-based techniques that can be used to analyze speciation and localization of NPs within the plant tissue: X-ray fluorescence (XRF) spectrometry and X-ray absorption (XAS) spectrometry. Both of them are based on measuring the spectra of emission or absorption of X-radiation. The absorption of X-ray photons by element is controlled by the photo-electric effect.

When sample is subjected to X-ray radiation, incident X-rays (photons) of a definite energy shine on the samples. If the energy of incident X-rays that reaches the sample is lower than the binding energy ( $E_0$ ) of the core electrons of the element, the atoms of this element do not participate in the absorption process. While with increasing energy of the incident X-ray photons, a point will be reached where their energy is approximately equal to the binding energy

of the core electrons. At this point a sharp increase in absorption of the X-ray photons occurs [27]. The energy absorbed by the core electron elevates it into a higher energy state or electron orbital, which is unoccupied. This excited core electron is referred to as a photoelectron. At the binding energy ( $E_0$ ), the photoelectron is ejected from the atom into the continuum [28]. As a result, a vacancy in the shell of the core electron is created in a core orbital. In order for the atom to return to the ground state, an electron from a higher energy orbital (e.g. L or M) fills the vacancy consequently, emitting X-ray photons in the form of fluorescence with characteristic energy corresponding to the difference between the two electronic levels' binding energies. These X-ray photons have characteristic energies for each element in the periodic table, confers element-specificity to the absorption and fluorescence spectroscopy.

During XRF process, the emitted fluorescence signal can be recorded at each position and used to generate XRF elemental maps. XRF is a nondestructive technique, it can be used to identify and determine the concentrations of elements present in biological samples, as well as providing information of in situ localization of elements in the samples.

During XAS process, the energy of the incident X-ray beam is progressively increased beyond the binding energy, thus the emission of fluorescence and absorption of the incident X-ray progressively increases, generating a characteristic X-ray absorption spectrum by detecting and recording the absorption or fluorescence at each energy point. The main feature of the XAS spectrum is a sharp, step-like curve called the absorption edge [28, 29].

The XAS spectrum is conventionally divided into two parts according to the energy region. The region comprising the pre-edge, the edge-jump and post-edge covering the energy range from approximately  $-50$  to  $+50$  eV of the absorption edge is defined as X-ray absorption near edge structure (XANES). The region from  $+50$  to  $+1000$  eV above the edge is defined as extended X-ray absorption fine structure (EXAFS) [28]. XANES is particularly sensitive to the oxidation states of elements and the electronegativity of the ligands, and it provides electronic structural information about the oxidation state and local geometry of the absorbing metal atom. EXAFS can provide information about the element coordination such as the identity and number of the coordinating atoms, and the interatomic distance between the central absorbing atom and its next nearest neighbors.

XAS is an element specific spectroscopic technique that provides specific qualitative information about chemical species at very high (subatomic) spatial resolution and is able to analyze almost any type of samples including amorphous (non-crystalline) materials in situ, requiring minor or no sample preparation prone to modify the chemical species. XAS experiments require an intense and polychromatic X-ray source. Synchrotron radiation is a very intense, collimated and polarized X-ray source, with a continuous band of wavelengths from around the  $\mu\text{m}$  (infrared) to the pm (hard X-ray) range [30]. Nowadays, owing to the development of synchrotron radiation facilities, the combination of synchrotron radiation with XAS is proved to be a powerful technique for speciation analysis of chemical elements.

XAS spectroscopy can be performed as bulk analyses to assess the overall speciation of the chemical of interest in the sample (usually homogenized). For bulk-XAS experiment, a beam in the size range of a few hundred  $\mu\text{m}^2$  to a few  $\text{mm}^2$  is used to illuminate sample, the XAS spectra obtained are generally representative of the average speciation of the chemical in the

sample [28, 31]. Whereas, the signal of minor species in the sample, which accounts for less than 5–10% of the total analyte, is insufficient to be resolved and quantified from the bulk spectra. In this case, bulk-XAS analysis is insufficient for us to obtain specific information from a complex and heterogeneous mixture of biological sample. This limitation can be overcome by decreasing the beam size to the range of tens of nm to a few  $\mu\text{m}$ , and using thin section of sample. This kind of laterally-resolved XAS analysis is referred to as  $\mu\text{-XAS}$ .

From  $\mu\text{-XAS}$  spectra, the information attained at each point of analysis is only representative of the spot probed and not of the overall speciation in the sample. Therefore, a trade-off exists between detecting minor species and obtaining the overall speciation of the analyte in the whole sample. A strategy to solve the problem is coupling bulk XAS analyses with laterally resolved techniques such as  $\mu\text{-XRF}$ ,  $\mu\text{-XAS}$  and  $\mu\text{-XRD}$ . In a typical work flow, laterally resolved  $\mu\text{-XRF}$  elemental maps are first collected to identify spots of interest, which are then further probed by  $\mu\text{-XAS}$  analysis [28].

Recently, a new approach termed XANES imaging has been developed with the capacity to analyze element speciation and full lateral distribution over large areas of sample. In a XANES imaging process, an elemental map of the sample will be firstly generated to identify interesting areas, then the  $\mu\text{-X-ray}$  fluorescence signals from the interesting areas are collected repeatedly over progressively increased incident X-ray energies and scan across the characteristic absorption edge of the target element. These resulting maps can be aligned and stacked, then the XANES spectra can be extracted from individual pixels or groups of pixels over regions of interest, eventually, the spatial distribution of both major and minor species within the sample will be obtained [28]. A detailed information regarding comparison among bulk-XANES,  $\mu\text{-XANES}$  and XANES imaging is provided in a review by Gräfe et al. [28].

#### 2.1.6. X-ray diffraction

X-ray diffraction (XRD) is a nondestructive technique for characterizing crystallographic structure or elemental composition of crystalline materials. It can reveal information about the crystal structure, crystalline phase, preferred crystal orientation (texture), average crystallite size and strain of materials. The constructive interference of a monochromatic beam of X-rays diffracted at specific angles from each set of lattice planes in the crystalline sample will produce X-ray diffraction peaks, intensities of which are determined by the distribution of atoms within the lattice, therefore, an X-ray diffraction pattern will be generated which reflects the periodic atomic arrangements in the sample.

For synchrotron-based X-ray diffraction (SR-XRD) technique, the high intensity and well-defined wavelength of the incident synchrotron radiation will generate a better resolution of diffraction peaks and make SR-XRD capable in detecting minor constituents in a sample [27]. In addition, XRD is capable of 20  $\mu\text{m}$  lateral resolution with minimal sample preparation requirements, can be used as a valuable complementary or alternative methods to XAS analysis. A limitation of this method is that it's not applicable for amorphous materials; it can only characterize crystalline samples.

### 2.1.7. X-ray computed microtomography

X-ray computed microtomography ( $\mu$ CT) uses X-ray to create cross-sections of a sample that can be used to produce three-dimensional digital images of the sample's internal structure at a micron level spatial resolution without destroying the original sample [32].

In an absorption-edge synchrotron radiation-based  $\mu$ CT process, a high flux, monochromatic X-ray beam passes through the sample, a scintillator converts the transmitted X-rays into visible light and the resulting absorption projection is captured by a photodetector to produce 2D radiographs. The sample is then rotated (or the X-ray source and detector are rotated about the object) by a small angle, a series of 2D X-ray absorption images is captured successively between  $0^\circ$  and  $180^\circ$ . Using mathematical principles of tomography, this series of images is then reconstructed to produce a 3D image, thus a 3D distribution of the element of interest within the sample is obtained [27, 32].

### 2.1.8. Scanning transmission X-ray microscopy

Scanning transmission X-ray microscopy (STXM) is a type of X-ray microscopy that allows in situ mapping of elements at high lateral resolution within a specimen. STXM uses a Fresnel zone plate to focus synchrotron soft X-ray absorption beamline into a small spot, the sample is placed at the focus of the zone plate and scanned by X-ray, then a film or charged coupled device detector is used to detect the transmitted X-rays intensity that pass through the specimen [33].

STXM-XAS, a technique that in-situ conditions of a XAS experiment with a STXM microscope, is capable of determining chemical speciation with a spatial resolution of 10–30 nm [34]. STXM-XAS can handle samples with thicknesses up to 20 micron at 1.5 keV, which makes it possible to study a wider and more flexible range of materials, including various plant tissues [33].

### 2.1.9. Nano secondary ion mass spectrometry

Secondary ion mass spectrometry (SIMS) uses an energetic ion beam to bombard a sample, particles from the top few atomic layers of the sample surface are then removed, resulting in the consequent liberation of ions, known as secondary ions. These secondary ions are then sorted on the basis of their energy in the instrument's electrostatic sector and later dispersed in a mass spectrometer to produce a map giving information about the elemental or molecular distribution within the sample [29, 35].

Nano secondary ion mass spectrometry (NanoSIMS) is a nanoscopic scale resolution chemical imaging mass spectrometer based on SIMS [35]. The main advantage of NanoSIMS over other SIMS is the ability to operate at high mass resolution, while maintaining both excellent signal transmission and high lateral resolution (down to 50 nm) with a low detection limit (mg/kg range). It is capable of measuring most elements in the periodic table, from hydrogen to uranium, as well as their different isotopes. These advantages of NanoSIMS make it one of the most powerful tools to quantitatively investigate elemental distribution in organisms at the cellular level [36, 37]. It is reported that Nano-SIMS has been used for the analyses of NPs in biological samples including plant tissue [36].

Technique	Information provided	Spatial resolution	Detection limit	Advantages	Limitations	Examples of application
TEM	Size, size distribution, shape, distribution, aggregation state, structure	>0.1 nm	mg/kg	High resolution, in vivo	Destructive, sample preparation, high vacuum condition, insensitive to light elements	Cucumber [54]
SEM	Size, size distribution, shape, distribution, aggregation state, structure	1 nm to 1 $\mu$ m	mg/kg	High resolution, in vivo	High vacuum, sample preparation, insensitive to light elements	<i>Eichhornia crassipes</i> [50]
STEM	Size, size distribution, shape, distribution, aggregation state, structure	<0.1 nm	mg/kg	Atomic resolution, analysis of low concentrations (ppm), in vivo	Sample preparation, insensitive to light elements	<i>Chlamydomonas reinhardtii</i> [36]
DLS	Size distribution, zeta potential, hydrodynamic diameter	3 nm- $\mu$ m		In situ and real-time measurement, rapid and simple analysis	Difficult to interpret heterogeneous size distributions, aggregates, dust particles can ruin the measurements on nanoparticles, multiple scattering and particle interactions in high concentrations, limited capability on polydisperse samples	<i>Capsicum annum</i> L. [47] Romaine lettuce [48]
EDS	Elemental composition, distribution			Nonquantitative analysis		
XAS	Oxidation state, elemental composition, structure	ppm	mg/kg	In vivo, minor species can be investigated	Cause beam damage artifacts	Cucumber [54]
XRF	Solid state speciation, quantitative bulk analysis, isotope ratios, morphology		mg/kg	Nondestructive, in vivo		<i>Landoltia punctata</i> [51]
XRD	Structure, size	1-3 wt%		Nondestructive		
$\mu$ CT	Distribution			In vivo, nondestructive, 3D visualization		Wheat [52]

Technique	Information provided	Spatial resolution	Detection limit	Advantages	Limitations	Examples of application
STXM	Size, shape, visualization	30 nm		In vivo, no sample preparation, nondestructive, liquid conditions		Cucumber [59]
NanoSIMS	Distribution, elemental composition, surface properties	50 nm		In vivo, high mass resolution, high lateral resolution	Destructive, difficult to analyze some elements with poor secondary ion yield, such as Zn, Cd, and Mn	<i>Chlamydomonas reinhardtii</i> [36]
ICP-OES	Elemental composition, concentration	Not available	µg/l	Quantitative analysis	Do not provide information on particle shape or diameter	Rice [53]
ICP-MS	Bulk elemental composition, number concentration, mass concentration	Not available	ng/l	Quantitative analysis, high sensitivity, low background signal, rapid and simple analysis	Do not provide information on particle shape or diameter, minimum particle size is limited by ICP-MS sensitivity, background and dissolved element content, narrow optimum range of particle number concentrations	<i>Arabidopsis thaliana</i> [49]
SP-ICP-MS	Concentration, number concentration, mass concentration	Not available	ng/l	Quantitative analysis, high sensitivity, low background signal, rapid and simple analysis	Do not provide information on particle shape or diameter, minimum particle size is limited by ICP-MS sensitivity, background and dissolved element content, narrow optimum range of particle number concentrations	Soybean and rice [55] <i>Arabidopsis thaliana</i> [44]

**Table 1.** Overview of analytical techniques discussed in this review with examples of application.

A limitation of NanoSIMS technique is that it is difficult to analyze elements with poor secondary ion yield, such as Zn, Cd, and Mn [37]. In addition, it is a destructive technique, which can be a disadvantage for some samples. This problem can be overcome by using high-pressure freezing followed by freeze substitution to preserve cellular and subcellular structures as well as elemental distributions of plant cells [29].

## 2.2. ICP-based techniques

### 2.2.1. Inductively coupled plasma-optical emission spectrometry

Inductively coupled plasma (ICP) based analytical techniques can provide quantitative elemental composition of a wide variety of sample types, including solids, liquids, and suspensions. Inductively coupled plasma-optical emission Spectrometry (ICP-OES) can be used to measure nanoparticle number concentration and elemental composition within a sample. As ICP-based techniques involve the use of liquid phases, suspensions could be analyzed directly, but solid samples have to be pretreated for the digestion of the matrix [21]. Generally, solid samples are dissolved or digested using acid in a microwave to get volatile analytic species. The sample solution is then nebulized into the core of inductively coupled argon plasma, where a flame temperature in a range from 6000 to 10,000 K vaporizes the nebulized solution, thus the analytic species are atomized, ionized and thermally excited. The excited atoms and ions return to low energy position, emitting electromagnetic radiation at wavelengths characteristic of a particular element, then the analytic species can be detected and quantified with an optical emission spectrometer (OES) through measuring the intensity of radiation, which is converted to elemental concentration by comparison with calibration standards.

### 2.2.2. Inductively coupled plasma-mass spectrometry

Inductively coupled plasma-mass spectrometry (ICP-MS) is an inorganic elemental analysis technique based on atomic mass spectrometry. ICP-MS consists of an ion source, a sampling interface, ion lens, a mass spectrophotometer and a detector system [18]. ICP sources are mainly used for metal analysis. It is an ideal ionization source for mass spectrometry, and can ionize over 90% of many elements. Mass spectrophotometer (e.g. ion trap, quadrupole or time-of-flight) covers different mass-to-charge ranges; differ in mass accuracy and achievable resolution.

During ICP-MS process, the ICP source is used to decompose, atomize and ionize a sample of interest. The ions generated in the high temperature argon plasma core are subsequently sorted by mass with the mass spectrophotometer and subjected to further elemental and isotopic analysis. The identities of the ions are determined by their mass-to-charge ratio using a mass analyzer, while the ions intensity is measured at ppt to ppm levels using the ion detector, then the intensity measurements are converted to elemental concentration by comparison with calibration standards. With the high sensitivity and specificity, ICP-MS has been widely used for the detection, characterization, and quantification of nanoparticles [38].

### 2.2.3. Single particle inductively coupled plasma-mass spectrometry

ICP-MS can be used in single particle mode to characterize individual particles, termed single particle inductively coupled plasma-mass spectrometry (SP-ICP-MS). During SP-ICP-MS

process, the sample is first suspended in a nebulized liquid and subsequently carried to argon plasma, where the sample is sequentially desolvated and atomized and ionized, creating a plume of ions. The ions pass through the mass spectrometer where they are separated by mass-to-charge ratio and detected using a time resolved analysis acquisition. The sample solution needs to be diluted sufficiently to ensure low concentrations (ppt to ppb) that no more than one particle will enter the plasma at a time. By using sufficiently short integration (dwell) time which is a duration for the instrument to take a reading, thousands of fast and individual readings are generated to capture nanoparticle event as a discrete signal pulse, each pulse is assumed to correlate to one nanoparticle event [39–41]. Based on ionic calibration standard, the particle mass can be determined by the intensity of the ICP-MS response. If the density of the elemental constituents of the particle is known, the theoretical size of the particle can be determined. If the transport efficiency from the nebulizer to the plasma is known, then the particle number concentration can be further calculated [38, 42].

SP-ICP-MS has been widely applied to measure particle size, size distribution, number concentration and elemental composition of nanoparticles in biological samples, demonstrating it as a powerful tool in quantifying NPs. To deal with biological tissues, a strong acid extraction procedure is required to release the NPs from the matrix. This introduces the possible dissolution of metal NPs which challenges the accuracy of the final analytical data. To solve this problem, Dan et al. studied recoveries of gold NPs when using such a special macerating enzyme that appeared to release the NPs from plant tissue without changing the size distribution of the NPs [43]. With the aid of enzymatic digestion, we have applied SP-ICP-MS analysis to characterize Ag NPs internalized by Arabidopsis, thus having established a new technique and opened up new research domain in our lab [44]. Overview of these analytical techniques including advantages and limitations with examples of application in plant-NP interaction studies is provided in **Table 1**.

### 3. Detection and characterization of nanoparticles in plants

Although a range of techniques are available to detect and characterize uptake, translocation and biotransformation of NPs in plant tissue, no single technique can provide all information regarding plant-NP interaction. Sufficient information is often obtained by the combination of these analytical techniques, which could provide complementary information mutually. Here in this section literature examples from recent studies are used to demonstrate the application of different techniques in the study of plant-NP interaction.

#### 3.1. Before NPs application

Careful characterization of NPs is critical for accurately assessing the impacts of nanoparticles on plants and understanding their behavior. When initiate an experiment, NPs will either diffuse or aggregate within certain biological media due to different characteristics of the media (i.e. pH, ionic strength, concentration and redox conditions) [45, 46], the aggregation state of NPs will result in quite distinct properties from original NPs. Therefore, the characterization of original NPs is often the first step before NPs application [45–47]. Zhang et al. used TEM images to observe the shape and size of nCeO<sub>2</sub> before applied to romaine lettuce. XRD spectrum confirmed the cubic

fluorite structure of  $n\text{CeO}_2$ ; then ICP-MS was used to confirm the purity of  $n\text{CeO}_2$ . Measuring zeta potential and hydrodynamic size of  $n\text{CeO}_2$  by DLS analysis indicated a significant aggregation of particles after mixing  $n\text{CeO}_2$  with nutrient solution. After  $n\text{CeO}_2$  application,  $\mu$ -XRF analysis showed that Ce mostly distributed outside the roots. TEM images confirmed that large amount of  $n\text{CeO}_2$  aggregates distributed on the root surface [48]. Yang et al. used TEM to measure averaged size of  $\text{CeO}_2$ -NPs suspended in deionized water, and XRD was employed to detect average primary particle size of  $\text{CeO}_2$ -NPs in dry powder samples, as well as to confirm the crystal structures of  $\text{CeO}_2$ -NPs [49]. Vinković et al. used DLS, TEM and ICP-MS to characterize AgNPs in ultrapure water (UPW) and sterilized tap water used for the plant watering (TWW) [47]. By measuring hydrodynamic diameter, zeta potential and polydispersity index (PdI) of citrate-coated AgNPs, DLS results showed that the volume size distribution in UPW was bimodal with 90% of smaller particles ( $12.9 \pm 9.1$  nm) and only 9% of bigger particles ( $87.6 \pm 41.7$  nm). The zeta potential value equal to  $-16.9 \pm 0.6$  mV indicated electrostatic stabilization of AgNPs in UPW. While after suspension in TWW, AgNPs aggregation occurred due to higher ionic strength of TWW. Further TEM analysis confirmed the presence of flocculated and aggregated AgNPs in TWW. ICP-MS was used to estimate the stability of AgNPs upon dissolution, results showed that total Ag was lower than 0.5% in TWW, which implies that  $\text{Ag}^+$  release was not occurred in TWW [47].

### 3.2. Uptake and translocation of NPs in plants

In order to understand the uptake mechanism of NPs and their translocation pathway, imaging techniques are often employed to visualize the distribution and morphology of NPs upon exposure, EDS can provide information on their chemical composition, while ICP-based techniques are used to measure particle number concentration, size distribution and mass concentration. Zhao et al. used SEM imaging to find that the root tip of *Eichhornia crassipes* after CuO NP exposure was thinner than unexposed root. EDS analysis of the aggregates attached on epidermis showed the presence of 37.6% (w/w) of Cu, confirmed that CuO NPs presented on the surface of root tips. Further through TEM imaging, dark aggregates with high electron density were detected in the intercellular spaces of cortical tissues in roots, and EDS analysis confirmed the presence of Cu on these aggregates, indicating that CuO NPs were taken up by roots and located in intercellular spaces [50]. Yang et al. used ICP-MS to find that  $\text{CeO}_2$ -NPs were taken up from root and subsequently translocated to shoot tissues in *Arabidopsis thaliana*, Ce accumulation was much higher in  $\text{CeO}_2$ -NP treatments than those in  $\text{CeO}_2$ -bulk and ionic Ce treatments, indicated that the toxicity resulted from the  $\text{CeO}_2$ -NPs per se rather than from the dissolved Ce ions. TEM images showed the presence of a large number of needle-like particle aggregations in the intercellular regions and the cytoplasm of leaf cells [49]. Stegemeier et al. used synchrotron-based  $\mu$ -XRF to visualize silver distribution in duckweed roots exposed to  $\text{Ag}^0$  NPs or  $\text{Ag}_2\text{S}$  NPs, or to  $\text{AgNO}_3$ . The silver  $K\alpha$  XRF maps showed clear differences in the distribution of Ag for each type of Ag used. The silver was distributed throughout the root tip and showed highest concentrations near the apical meristem after exposure to  $\text{AgNO}_3$ . A similar distribution of Ag in root tip was shown after exposure to  $\text{Ag}^0$ -NPs. While after exposure to  $\text{Ag}_2\text{S}$ -NPs, a hotspot of silver located at the end of the root cap, suggested that silver was not readily internalized in this case [51]. Pradas del Real et al. firstly used  $\mu$ -CT to create 3D reconstructed image of wheat root after Ag NPs exposure for in situ 3D visualization, then  $\mu$ -XRF was used to provide 2D elemental distribution [52]. Combination of  $\mu$ -CT and  $\mu$ -XRF showed the presence of localized Ag accumulation regions with a size of 1–4  $\mu\text{m}$  adhering on the epidermis. Nano-CT technique capable of higher spatial resolution revealed that these

AgNPs accumulated preferentially in discontinuities between root epidermal cells. In addition, many AgNPs were fixed on root hairs. With the methods to study Ag<sub>2</sub>S-NPs treatment,  $\mu$ -XRF showed that Ag is mainly colocalized with S,  $\mu$ -CT and nano-CT showed that these Ag accumulation regions with a size from 3 to 8  $\mu$ m presented mostly on the root surface. Through ICP-MS analysis, a higher Ag content in root and shoot was observed after exposure to AgNPs compared to AgNO<sub>3</sub> exposure, suggesting a nano-specific accumulation mechanism [52]. Peng et al. used ICP-OES to measure Cu content in root of rice after adding CuO NPs to the soil. The results showed that Cu content in roots was significantly increased, with a much higher content than aboveground parts.  $\mu$ -XRF analysis indicated that Cu accumulated in the aleuronic layer of rice, but not the polished rice [53]. In another study, In order to study whether CeO<sub>2</sub> NPs can move from the roots to shoots in cucumber after the root was exposed to CeO<sub>2</sub> NPs, TEM and EDS analyses were performed and the presence of Ce particles in the xylem sap was confirmed, suggested that Ce-containing species could be transported throughout the whole plant by vascular system. ICP-MS analysis also confirmed the uptake of CeO<sub>2</sub> NPs from root to shoot [54]. Li et al. used the macerozyme R-10 tissue extraction method followed by SP-ICP-MS to study the uptake and size distribution of AgNPs in soybean and rice. Both SP-ICP-MS and TEM measurements indicated that the size of Ag-containing NPs were 2–3 times larger than the originally dosed AgNPs after exposure to AgNPs, indicating the AgNPs biotransformation processes were involved [55].

### 3.3. Biotransformation of NPs in plants

Biotransformation is defined as biochemical modification by living organisms [16, 56]. Biotransformation of NPs by plant may modify the toxicity, behavior, and fate of NPs in the plant tissue. Biotransformation process may involve redox, dissolution, sulfidation, aggregation, and adsorption of macromolecules and ion [10, 57]. XAS and STXM are the most frequently used techniques to characterize the speciation of NPs during cellular internalization and intracellular biotransformation. Zhao et al. used EDS technique to find that S present on aggregates in the intercellular spaces of cortical tissues in *Eichhornia crassipes* (water hyacinth) roots after CuO NP exposure, indicating that CuO NPs (or other Cu species) interacted with S-containing compounds such as cysteine. XANES was employed to identify Cu species in roots and leaves after CuO NPs internalization. XANES analysis revealed that CuO NPs in roots mainly kept the original pattern (65.7% of CuO). Other Cu species included Cu-Ac (14.2%), Cu<sub>2</sub>(OH)PO<sub>4</sub> (8.7%) and 7.6% of Cu<sub>2</sub>S. XRD spectrum of original CuO NPs showed that all peaks belonged to CuO, and no peak on Cu<sub>2</sub>S was detected, indicating that the observed Cu<sub>2</sub>S in roots were formed after incubation with CuO NPs [50]. Zhang et al. used Bulk-XANES technique to study transformation of nCeO<sub>2</sub>. XANES spectra of root and shoot showed similar feature as the initial nCeO<sub>2</sub>; Results showed that Ce in lettuce mostly presented as CeO<sub>2</sub>, with a small fraction of CePO<sub>4</sub> in roots (4.3%) and Ce carboxylates (3.5%) in leaves, suggested that nCeO<sub>2</sub> can release small amount of Ce<sup>3+</sup> with the assistance of organic acids and reducing substances in root exudates [48, 58]. Stegemeier et al. used EXAFS spectra to determine Ag speciation in duckweed (*Landoltia punctata*) roots after exposure to Ag<sup>0</sup> NPs or Ag<sub>2</sub>S NPs, or AgNO<sub>3</sub>, revealed that more photo-reducible Ag species were generated after exposure to ionic Ag [51]. In contrast, a higher prevalence of sulfur associated Ag species (as a mixture of Ag<sub>2</sub>S (64%) and Ag-thiol (53%)) were produced after exposure to Ag<sup>0</sup> NPs or Ag<sub>2</sub>S NPs treatment. Bulk EXAFS analysis of Ag<sub>2</sub>S-NP treatment indicated that plant is unable to dissolve or transform a significant amount of the Ag<sub>2</sub>S-NPs after 24 h exposure [51]. In another study,  $\mu$ -XANES spectroscopy was employed to determine speciation of Ag at root after Ag NPs exposure.

$\mu$ -XANES revealed that Ag was mostly present as metallic Ag in the epidermis, but inside the roots Ag was homogeneously distributed in the cell walls of the cortex as a mixture of Ag-thiol species and other ionic Ag species, suggested the biotransformation of Ag occurred. Moreover, no Ag(0) was observed inside roots, implied that Ag-NPs were completely dissolved and complexed by organic ligands [52]. Peng et al. used Bulk-XANES to analyze translocation and transformation of CuO NPs in rice, the results revealed that Cu element mainly existed in the form of copper citrate, only a small portion of Cu kept original CuO form in roots, stems, and leaves of rice after CuO NP treatment. During CuO NPs internalization in rice, one-third of Cu(II) was transformed to Cu(I) which was mainly associated with cysteine. CuO, copper citrate, and copper (I) acetate all accounted for nearly 30% of the total Cu in the chaff [53]. Ma et al. combined  $\mu$ -XRF and  $\mu$ -XANES to detect CeO<sub>2</sub> NPs or its transformation species in the xylem sap, shoots and roots of cucumber after exposure to CeO<sub>2</sub> NPs, revealed that about 15% of Ce was reduced from Ce(IV) to Ce(III) in the roots after treatment, and Ce was transported as a mixture of Ce(IV) and Ce(III) from roots to shoots through xylem, while was transported almost only in the form of CeO<sub>2</sub> from shoots back to roots through phloem [54]. Peng et al. used bulk-XANES to analyze Cu speciation in the tissues of rice plants after exposure to CuP NPs, indicated that Cu was combined with cysteine, citrate, and phosphate ligands, and some of the Cu (II) was transformed to Cu (I) during CuO NP uptake, and confirmed that CuO NPs were transported from the roots to the leaves. In order to further study Cu biotransformation in cellular level, they firstly used  $\mu$ -XRF to map Cu element distribution in the root; the results revealed that Cu was mainly localized in the root epidermis and exodermis. Then  $\mu$ -XANES was employed to determine speciation of Cu element at selected spots in  $\mu$ -XRF map. In addition, combination of STXM with Cu L3-edge XANES spectroscopy was used to map the in situ elemental composition of Cu in the root cells, the results confirmed that speciation of Cu in the root cells and the intercellular space existed in the form of Cu-citrate and CuO NPs, respectively [10]. Zhang et al. used TEM to detect the uptake and localization of nano-Yb<sub>2</sub>O<sub>3</sub> in cucumber roots after exposure, found that a lot of high electron-dense dark deposits looked like fine needle-shaped nanoclusters in the intercellular spaces and middle lamellas in the cross sections of cucumber roots, later EDS analysis confirmed the presence of Yb in these dark deposits. In order to identify the chemical species of Yb in these dark deposits, the chemical distribution was mapped by STXM, and NEXAFS spectra were extracted, results indicated that this compound was inferred to be YbPO<sub>4</sub>, suggesting that Yb<sub>2</sub>O<sub>3</sub> particles and YbCl<sub>3</sub> were all transformed to YbPO<sub>4</sub> in the intercellular regions of the roots, and indicating that biotransformation and internalization of Yb<sub>2</sub>O<sub>3</sub> nanoparticle took place in plant cell, which conferred phytotoxicity to plant [59]. In another study, Zhang et al. used the same methodology to investigate the biotransformation of CeO<sub>2</sub> NPs in cucumber. TEM images showed the presence of needle-like clusters on the epidermis and in the intercellular spaces of cucumber roots after CeO<sub>2</sub> NPs exposure. STXM imaging indicated that the chemical composition of needle-like clusters is CePO<sub>4</sub>. Further XANES analysis showed that Ce presented in the roots as CeO<sub>2</sub> and CePO<sub>4</sub> while in the shoots as CeO<sub>2</sub> and cerium carboxylates, confirming biotransformation of CeO<sub>2</sub> NPs in plant cells [16]. In order to determine the toxicity and fate of nanoparticles upon exposure to plants, Wang et al. combined a variety of techniques to investigate the cellular internalization and intracellular biotransformation of silver nanoparticles in *Chlamydomonas reinhardtii*. NanoSIMS was firstly applied to analyze the distributions of Ag in algal cells, silver was observed to accumulate predominantly on the cell walls and in the cytoplasm of the algae after exposure to AgNPs. Then HAADF-STEM was performed to examine the accurate localization and morphology of Ag, HAADF image showed that a set of bright spots

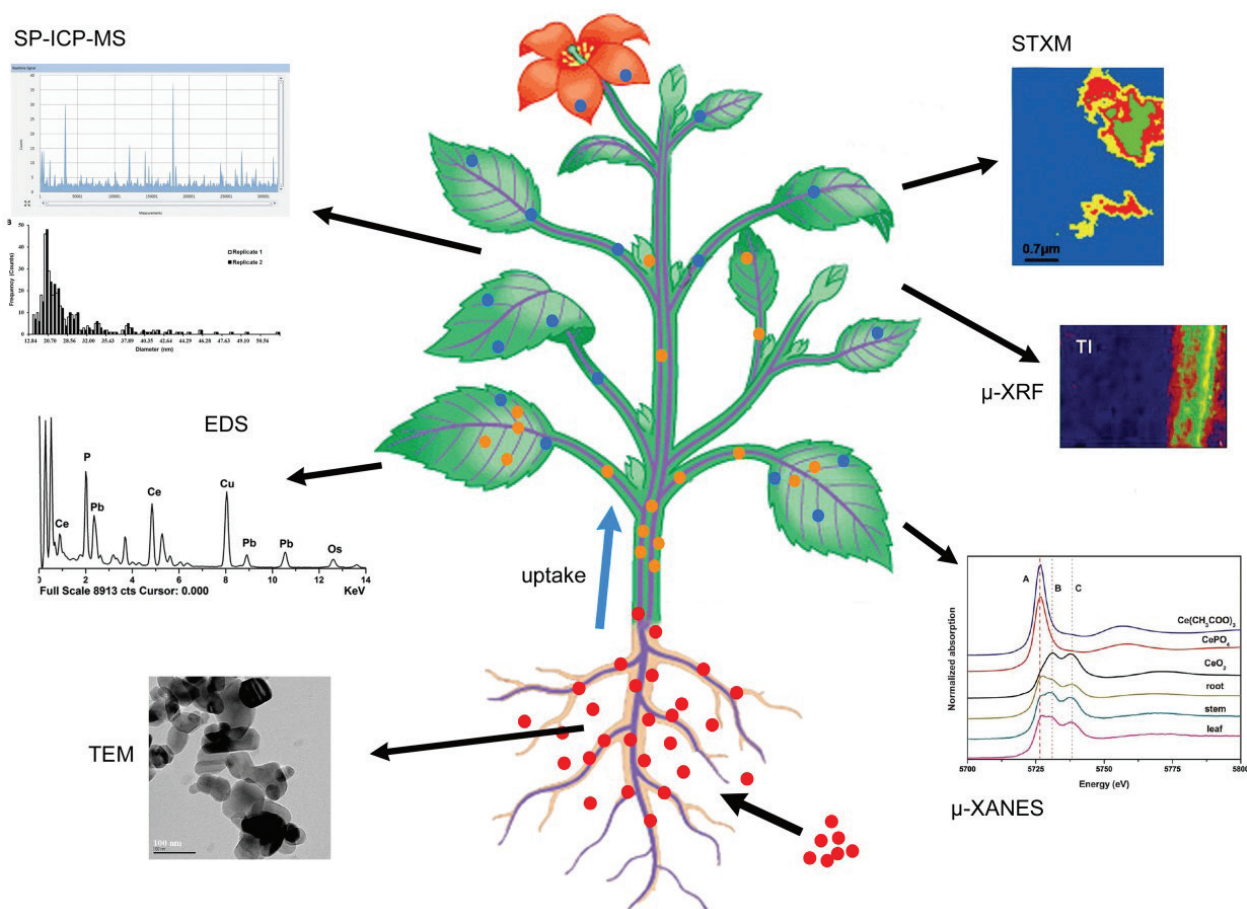


**Figure 1.** Schematic diagram represent a regular work flow of NPs characterization in plant. A selection of analytical techniques is shown. Red dots indicate NPs at the moment of application. Yellow and blue dots indicate different elemental species of NPs after biotransformation in plants. The images of SP-ICP-MS, EDS, TEM, STXM, μ-XRF and μ-XANES are adapted from [16, 18, 44, 60].

located mainly in the periplasmic space and cytoplasm, TEM was further used to observe morphology of these bright spots. EDS analysis showed that these bright spots were Ag-containing substances; moreover, Ag and S always occurred concomitantly. EDS-mapping confirmed that Ag was almost exclusively co-localized with S in the cytoplasm of algae but not in the periplasmic space. Later, Synchrotron based Ag K-edge XAS was performed to further identify Ag speciation after exposure. It was found that Ag glutathione complexes and  $Ag_2S$  represented the main speciation, suggested that Silver was also found to coexist with sulfur inside the cytoplasm in the form of Ag-GSH and  $Ag_2S$  [36]. A regular work flow of NPs characterization during plant-NP interaction with the application of the most-frequently used techniques is shown in **Figure 1**.

#### 4. Conclusion and future perspectives

Although the combination of these techniques described in this review is capable of taking over most of the task on the characterization of NPs during plant-NP interaction, considerable limitations of these techniques still remain to overcome. Many techniques are destructive, such as TEM, SEM and nanoSIMS, which means the same sample cannot be analyzed twice or by another method for validation. Analytical artifacts are sometimes inevitable during some sample preparation

procedures. Because biological samples is usually hetero-dispersed and multicomponent, with diverse elemental compositions and sometimes contain multiple types of NPs, the analysis of NPs in these samples is thus quite complicated and a variety of methodology is utilized to provide complementary information, while the results measured by these different methods are not always comparable, which may partially due to different sample preparation procedures in different techniques. Further, instrument operation procedures and statistical analyses are likely to contribute to the complexity and uncertainty. Another challenge arises when analyze samples with low concentrations of the analyte. In non-hyperaccumulating plant species, visualizing the spatial distribution of NPs and detecting reliable in situ information about the chemical speciation of trace elements will be very difficult. In this case, analytical techniques with high sensitivity are desired to measure low concentrations of NPs. An ideal analytical technique should be able to simultaneously determine all parameters regarding plant-NP interaction, such as particle size, morphology, structure, size distribution, mass concentration, translocation, elemental speciation and etc. It should be sensitive and accurate enough for in situ detection and characterization of trace element in complex biological samples in a non-destructive way. Although none of the existing techniques are able to solely provide all the information desired, we believe that a promising evolution of analytical methodology is taking place and will be capable of fulfilling requirements as much as desired to provide sufficient information about plant-NP interaction.

## Acknowledgements

Authors thank the NIE AcRF grant (RI 8/16 CZ).

## Conflict of interest

Authors declare no conflict of interest.

## Abbreviations

DLS	dynamic light scattering
EDS	energy-dispersive X-ray spectroscopy
EXAFS	extended X-ray absorption fine structure
ICP-MS	inductively coupled plasma-mass spectrometry
ICP-OES	inductively coupled plasma-optical emission spectrometry
NanoSIMS	nano secondary ion mass spectrometry
NPs	nanoparticles
SEM	scanning electron microscope
SP-ICP-MS	single particle-inductively coupled plasma-mass spectrometry

STEM	scanning transmission electron microscope
STXM	scanning transmission X-ray microscopy
TEM	transmission electron microscope
XANES	X-ray absorption near edge structure
XAS	X-ray absorption spectrometry
XRD	X-ray diffraction
XRF	X-ray fluorescence spectrometry
$\mu$ CT	X-ray computed microtomography

## Author details

An Yan and Zhong Chen\*

\*Address all correspondence to: [zhong.chen@nie.edu.sg](mailto:zhong.chen@nie.edu.sg)

Natural Sciences and Science Education Academic Group, National Institute of Education,  
Nanyang Technological University, Singapore

## References

- [1] Sekhon BS. Nanotechnology in agri-food production: An overview. *Nanotechnology, Science and Applications*. 2014;**7**:31-53
- [2] Nel A, Xia T, Mädler L, Li N. Toxic potential of materials at the nanolevel. *Science*. 2006;**311**:622-627
- [3] Zhu H, Han J, Xiao JQ, Jin Y. Uptake, translocation, and accumulation of manufactured iron oxide nanoparticles by pumpkin plants. *Journal of Environmental Monitoring*. 2008;**10**:713-717
- [4] Handy RD, Owen R, Valsami-Jones E. The ecotoxicology of nanoparticles and nanomaterials: Current status, knowledge gaps, challenges, and future needs. *Ecotoxicology*. 2008;**17**:315-325
- [5] Ma X, Geiser-Lee J, Deng Y, Kolmakov A. Interactions between engineered nanoparticles (ENPs) and plants: Phytotoxicity, uptake and accumulation. *Science of the Total Environment*. 2010;**408**:3053-3061
- [6] Wang P, Lombi E, Zhao F-J, Kopittke PM. Nanotechnology: A new opportunity in plant sciences. *Trends in Plant Science*. 2016;**21**:699-712
- [7] Dietz K-J, Herth S. Plant nanotoxicology. *Trends in Plant Science*. 2011;**16**:582-589
- [8] Miralles P, Church TL, Harris AT. Toxicity, uptake, and translocation of engineered nanomaterials in vascular plants. *Environmental Science & Technology*. 2012;**46**:9224-9239

- [9] Judy JD, Bertsch PM. Chapter one—Bioavailability, toxicity, and fate of manufactured nanomaterials in terrestrial ecosystems. In: Sparks DL, editor. *Advances in Agronomy*. United States: Academic Press; 2014. pp. 1-64
- [10] Peng C, Duan D, Xu C, Chen Y, Sun L, et al. Translocation and biotransformation of CuO nanoparticles in rice (*Oryza sativa* L.) plants. *Environmental Pollution*. 2015;**197**:99-107
- [11] Stampoulis D, Sinha SK, White JC. Assay-dependent phytotoxicity of nanoparticles to plants. *Environmental Science & Technology*. 2009;**43**:9473-9479
- [12] Auffan M, Rose J, Bottero J-Y, Lowry GV, Jolivet J-P, et al. Towards a definition of inorganic nanoparticles from an environmental, health and safety perspective. *Nature Nanotechnology*. 2009;**4**:634-641
- [13] Gardea-Torresdey JL, Rico CM, White JC. Trophic transfer, transformation, and impact of engineered nanomaterials in terrestrial environments. *Environmental Science & Technology*. 2014;**48**:2526-2540
- [14] Geisler-Lee J, Brooks M, Gerfen J, Wang Q, Fotis C, et al. Reproductive toxicity and life history study of silver nanoparticle effect, uptake and transport in *Arabidopsis thaliana*. *Nanomaterials*. 2014;**4**:301
- [15] Montes A, Bisson MA, Gardella JA, Aga DS. Uptake and transformations of engineered nanomaterials: Critical responses observed in terrestrial plants and the model plant *Arabidopsis thaliana*. *Science of the Total Environment*. 2017;**607-608**:1497-1516
- [16] Zhang P, Ma Y, Zhang Z, He X, Zhang J, et al. Biotransformation of ceria nanoparticles in cucumber plants. *ACS Nano*. 2012;**6**:9943-9950
- [17] Chau C-F, Wu S-H, Yen G-C. The development of regulations for food nanotechnology. *Trends in Food Science & Technology*. 2007;**18**:269-280
- [18] Tiede K, Boxall ABA, Tear SP, Lewis J, David H, et al. Detection and characterization of engineered nanoparticles in food and the environment. *Food Additives & Contaminants: Part A*. 2008;**25**:795-821
- [19] Stokes D. *Principles and Practice of Variable Pressure: Environmental Scanning Electron Microscopy (VP-ESEM)*. United States: John Wiley & Sons; 2008
- [20] Akbari B, Pirhadi Tavandashti M, Zandrahimi M. Particle size characterization of nanoparticles—A practical approach. *Iranian Journal of Materials Science & Engineering*. 2011;**8**:48-56
- [21] Laborda F, Bolea E, Cepriá G, Gómez MT, Jiménez MS, et al. Detection, characterization and quantification of inorganic engineered nanomaterials: A review of techniques and methodological approaches for the analysis of complex samples. *Analytica Chimica Acta*. 2016;**904**:10-32
- [22] Hendrickson OD, Safenkova IV, Zherdev AV, Dzantiev BB, Popov VO. Methods of detection and identification of manufactured nanoparticles. *Biophysics*. 2011;**56**:961-986
- [23] Liu J. Scanning transmission electron microscopy and its application to the study of nanoparticles and nanoparticle systems. *Journal of Electron Microscopy*. 2005;**54**:251-278

- [24] Kim B, Park C-S, Murayama M, Hochella MF. Discovery and characterization of silver sulfide nanoparticles in final sewage sludge products. *Environmental Science & Technology*. 2010;**44**:7509-7514
- [25] Brar SK, Verma M. Measurement of nanoparticles by light-scattering techniques. *TrAC Trends in Analytical Chemistry*. 2011;**30**:4-17
- [26] Goldstein JI, Newbury DE, Michael JR, Ritchie NW, Scott JHJ, et al. *Scanning Electron Microscopy and X-Ray Microanalysis*. Germany: Springer; 2017
- [27] Lombi E, Susini J. Synchrotron-based techniques for plant and soil science: Opportunities, challenges and future perspectives. *Plant and Soil*. 2009;**320**:1-35
- [28] Gräfe M, Donner E, Collins RN, Lombi E. Speciation of metal(loid)s in environmental samples by X-ray absorption spectroscopy: A critical review. *Analytica Chimica Acta*. 2014;**822**:1-22
- [29] Zhao F-J, Moore KL, Lombi E, Zhu Y-G. Imaging element distribution and speciation in plant cells. *Trends in Plant Science*. 2014;**19**:183-192
- [30] Ortega R, Carmona A, Llorens I, Solari PL. X-ray absorption spectroscopy of biological samples: A tutorial. *Journal of Analytical Atomic Spectrometry*. 2012;**27**:2054-2065
- [31] Manceau A, Boisset M-C, Sarret G, Hazemann J-L, Mench M, et al. Direct determination of lead speciation in contaminated soils by EXAFS spectroscopy. *Environmental Science & Technology*. 1996;**30**:1540-1552
- [32] Landis EN, Keane DT. X-ray microtomography. *Materials Characterization*. 2010;**61**:1305-1316
- [33] de Groot FMF, de Smit E, van Schooneveld MM, Aramburo LR, Weckhuysen BM. In-situ scanning transmission X-ray microscopy of catalytic solids and related nanomaterials. *Chemphyschem*. 2010;**11**:951-962
- [34] Bluhm H, Andersson K, Araki T, Benzerara K, Brown GE, et al. Soft X-ray microscopy and spectroscopy at the molecular environmental science beamline at the advanced light source. *Journal of Electron Spectroscopy and Related Phenomena*. 2006;**150**:86-104
- [35] Herrmann AM, Ritz K, Nunan N, Clode PL, Pett-Ridge J, et al. Nano-scale secondary ion mass spectrometry – A new analytical tool in biogeochemistry and soil ecology: A review article. *Soil Biology and Biochemistry*. 2007;**39**:1835-1850
- [36] Wang S, Lv J, Ma J, Zhang S. Cellular internalization and intracellular biotransformation of silver nanoparticles in *Chlamydomonas reinhardtii*. *Nanotoxicology*. 2016;**10**:1129-1135
- [37] Moore KL, Lombi E, Zhao F-J, Grovenor CRM. Elemental imaging at the nanoscale: NanoSIMS and complementary techniques for element localisation in plants. *Analytical and Bioanalytical Chemistry*. 2012;**402**:3263-3273
- [38] Wilbur S, Yamanaka M, Sannac S. *Characterization of Nanoparticles in Aqueous Samples by ICP-MS*. United States: Agilent Publication; 2015

- [39] Mitrano D, Ranville J, Stephan C, Shelton C (2014) Quantitative Evaluation of Nanoparticle Dissolution Kinetics Using Single Particle ICP-MS: A Case Study with Silver Nanoparticles. PerkinElmer application note
- [40] Mitrano DM, Leshner EK, Bednar A, Monserud J, Higgins CP, et al. Detecting nanoparticulate silver using single-particle inductively coupled plasma-mass spectrometry. *Environmental Toxicology and Chemistry*. 2012;**31**:115-121
- [41] Pace HE, Rogers NJ, Jarolimek C, Coleman VA, Gray EP, et al. Single particle inductively coupled plasma-mass spectrometry: A performance evaluation and method comparison in the determination of nanoparticle size. *Environmental Science & Technology*. 2012;**46**:12272-12280
- [42] Pace HE, Rogers NJ, Jarolimek C, Coleman VA, Higgins CP, et al. Determining transport efficiency for the purpose of counting and sizing nanoparticles via single particle inductively coupled plasma mass spectrometry. *Analytical Chemistry*. 2011;**83**:9361-9369
- [43] Dan Y, Zhang W, Xue R, Ma X, Stephan C, et al. Characterization of gold nanoparticle uptake by tomato plants using enzymatic extraction followed by single-particle inductively coupled plasma-mass spectrometry analysis. *Environmental Science & Technology*. 2015;**49**:3007-3014
- [44] Bao D, Oh ZG, Chen Z. Characterization of silver nanoparticles internalized by *Arabidopsis* plants using single particle ICP-MS analysis. *Frontiers in Plant Science*. 2016;**7**:32
- [45] Vinkovic Vrcek I, Pavicic I, Crnkovic T, Jurasin D, Babic M, et al. Does surface coating of metallic nanoparticles modulate their interference with in vitro assays? *RSC Advances*. 2015;**5**:70787-70807
- [46] Auffan M, Rose J, Wiesner MR, Bottero J-Y. Chemical stability of metallic nanoparticles: A parameter controlling their potential cellular toxicity in vitro. *Environmental Pollution*. 2009;**157**:1127-1133
- [47] Vinković T, Novák O, Strnad M, Goessler W, Jurašin DD, et al. Cytokinin response in pepper plants (*Capsicum annuum* L.) exposed to silver nanoparticles. *Environmental Research*. 2017;**156**:10-18
- [48] Zhang P, Ma Y, Liu S, Wang G, Zhang J, et al. Phytotoxicity, uptake and transformation of nano-CeO<sub>2</sub> in sand cultured romaine lettuce. *Environmental Pollution*. 2017;**220**:1400-1408
- [49] Yang X, Pan H, Wang P, Zhao F-J. Particle-specific toxicity and bioavailability of cerium oxide (CeO<sub>2</sub>) nanoparticles to *Arabidopsis thaliana*. *Journal of Hazardous Materials*. 2017;**322**:292-300
- [50] Zhao J, Ren W, Dai Y, Liu L, Wang Z, et al. Uptake, distribution, and transformation of CuO NPs in a floating plant *Eichhornia crassipes* and related stomatal responses. *Environmental Science & Technology*. 2017;**51**:7686-7695
- [51] Stegemeier JP, Colman BP, Schwab F, Wiesner MR, Lowry GV. Uptake and distribution of silver in the aquatic plant *Landoltia punctata* (duckweed) exposed to silver and silver sulfide nanoparticles. *Environmental Science & Technology*. 2017;**51**:4936-4943

- [52] Pradas del Real AE, Vidal V, Carrière M, Castillo-Michel H, Levard C, et al. Silver nanoparticles and wheat roots: A complex interplay. *Environmental Science & Technology*. 2017;**51**:5774-5782
- [53] Peng C, Xu C, Liu Q, Sun L, Luo Y, et al. Fate and transformation of CuO nanoparticles in the soil–rice system during the life cycle of rice plants. *Environmental Science & Technology*. 2017;**51**:4907-4917
- [54] Ma Y, He X, Zhang P, Zhang Z, Ding Y, et al. Xylem and phloem based transport of CeO<sub>2</sub> nanoparticles in hydroponic cucumber plants. *Environmental Science & Technology*. 2017;**51**:5215-5221
- [55] Li C-C, Dang F, Li M, Zhu M, Zhong H, et al. Effects of exposure pathways on the accumulation and phytotoxicity of silver nanoparticles in soybean and rice. *Nanotoxicology*. 2017;**11**:699-709
- [56] Abramowicz DA. Aerobic and anaerobic biodegradation of PCBs: A review. *Critical Reviews in Biotechnology*. 1990;**10**:241-251
- [57] Lowry GV, Gregory KB, Apte SC, Lead JR. Transformations of nanomaterials in the environment. *Environmental Science & Technology*. 2012;**46**:6893-6899
- [58] Zhang P, Ma Y, Zhang Z, He X, Li Y, et al. Species-specific toxicity of ceria nanoparticles to *Lactuca* plants. *Nanotoxicology*. 2015;**9**:1-8
- [59] Zhang P, Ma Y, Zhang Z, He X, Guo Z, et al. Comparative toxicity of nanoparticulate/bulk Yb<sub>2</sub>O<sub>3</sub> and YbCl<sub>3</sub> to cucumber (*Cucumis sativus*). *Environmental Science & Technology*. 2012;**46**:1834-1841
- [60] Scheckel KG, Lombi E, Rock SA, McLaughlin MJ. In vivo synchrotron study of thallium speciation and compartmentation in *Iberis intermedia*. *Environmental Science & Technology*. 2004;**38**:5095-5100

IntechOpen

